Author Manuscript

Title: Self-Sacrificial Template-Directed Synthesis of Metal-Organic Framework-Derived Porous Carbon for Energy-Storage Devices

Authors: Bing Ding; Jie Wang; Zhi Chang; Guiyin Xu; Xiaodong Hao; Laifa Shen; Hui Dou; Xiaogang Zhang

This is the author manuscript accepted for publication and has undergone full peer review but has not been through the copyediting, typesetting, pagination and proofreading process, which may lead to differences between this version and the Version of Record.

To be cited as: ChemElectroChem 10.1002/celc.201500536

Link to VoR: http://dx.doi.org/10.1002/celc.201500536

WILEY-VCH

DOI: 10.1002/ ((please add manuscript number))
Article type: (**Full Paper**)

Self-Sacrificial Template-Directed Synthesis of Metal–Organic Framework-Derived Porous Carbon for Energy-Storage Devices

*Bing Ding, Jie Wang, Zhi Chang, Guiyin Xu, Xiaodong Hao, Laifa Shen, Hui Dou, and Xiaogang Zhang**

B. Ding, J. Wang, Z. Chang, G. Y. Xu, X. D. Hao, Dr. L. F. Shen, Prof. H. Dou, Prof. X. G. Zhang
Jiangsu Key Laboratory of Materials and Technology for Energy Conversion, College of Material Science and Engineering, Nanjing University of Aeronautics and Astronautics, Nanjing, 210016, P. R. China
E-mail: azhangxg@nuaa.edu.cn

Keywords: two-dimensional carbon, hierarchical porosity, metal–organic framework, self-sacrificial template, electrochemistry

Metal–organic frameworks (MOF)-derived carbon materials exhibit large surface area, but dominant micropore characteristic and uncontrollable dimension. Herein, we propose a self-sacrificial template-directed synthesis method to engineer the porous structure and dimension of MOF-derived carbon materials. Porous zinc oxide (ZnO) nanosheets solid is selected as the self-sacrificial template and two-dimensional (2D) nanostructure-directing agent to prepare 2D ZIF-8-derived carbon nanosheets (ZCNs). The as-prepared ZCNs materials exhibit large surface area with hierarchical porosity. These intriguing features render ZCNs materials advanced electrode materials for electrochemical energy-storage devices, demonstrating large ion-accessible surface area and high ion/electron transport rate. This self-sacrificial template-directed synthesis method offers new avenues for rational engineering the porous structure and dimension of MOF-derived porous carbon materials, thus exploiting their full potential for electrochemical energy-storage devices.

1. Introduction

Porous carbon materials, due to their appealing properties of large surface area, high electric conductivity, and excellent chemical stability, show broad range of applications in

This article is protected by copyright. All rights reserved

Author Manuscript

electrochemical energy-storage devices, including supercapacitors and batteries.[1] To develop high-performance electrode, various carbon materials with desired porous structures and morphologies have been extensively studied over the past few decades. [2] Recently, metal–organic framework (MOF)-derived carbon materials have emerged as promising candidates due to their unique characterizations.[3] MOF-derived carbon materials are prepared by direct pyrolysis of MOFs without any additional carbon sources or further activation. Because of the highly uniform pores and designable organic species in MOFs, MOF-derived carbon materials usually exhibit large surface area. To date, various MOF-derived carbon materials have been prepared from multiple types of MOFs.[3b,3c,4] For example, direct pyrolysis of commercially available $Zn(MeIm)_2$ (ZIF-8; MeIm= 2-methylimidazole) powder or ZIF-8 microcrystals could obtain porous carbon materials with Brunauer–Emmett–Teller (BET) surface areas up to 800–1610 $m^2 g^{-1}$.[4b,4d,4f-h] When used as the electrode material for supercapacitors, the specific capacitance achieve 130 F g^{-1} in aqueous electrolyte.[4b] ZIF-8-derived carbon materials are also potential sulfur immobilizer for lithium–sulfur (Li–S) batteries, which could confine sulfur species to improve the specific capacity and cycling stability of sulfur electrode.[4g-i]

Although the advantages of MOF-derived carbon materials for energy-storage applications have been highlighted a lot in previous reports, they still suffer from some drawbacks. Firstly, as electrode materials for electrochemical energy-storage devices, carbon materials with hierarchical porosity, typically mesopores in combination with micropores or macropores, are highly desirable.[5] MOF-derived carbon materials, however, normally exhibit dominant micropore characteristic, which limits ion diffusion and thus lowers the electrochemical performance, especially at high current density. Secondly, the dimension of carbon materials is vital to the electrolyte permeability and ion/electron transport kinetics.[6] For instance, two-dimensional (2D) carbon with high aspect ratio satisfies the requirements and manifest superior electrochemical performance.[7] In previous reports, great efforts have

This article is protected by copyright. All rights reserved

Author Manuscript

been devoted to synthesize MOFs microcrystals or nanocrystals precursor, but rational control on the dimension and porous structure of MOF-derived carbon are lacked. It is still a challenge to control the dimension of MOF-derived carbon materials, especially synthesis of 2D MOF-derived carbon. Recently, template-assistant strategy was developed to address the challenges of MOF-derived carbon.[8] Yu *et al.* described a tellurium nanowires-derived templating synthesis of ZIF-8 nanofibers and ZIF-8 nanofiber-derived carbon nanofibers.[8a] The carbon nanofibers exhibited a large specific area of 2270 m^2 g^{-1} and excellent performances for oxygen reduction reaction.[30] However, the high production costs and limited scalability of template restricts the wide application of MOF-derived carbon materials. In addition, to confine the growth of MOFs on the surface, some templates needs further surface modification.[8b, 8c]

An alternative strategy is self-sacrificing template method which fabricates desired nanostructure through sacrificing template themselves and initiating the growth process without any surface modification.[9] Inspired by this, a self-sacrificial template-directed synthesis method was proposed to engineer the porous structure and dimension of MOF-derived carbon material. In this work, for the convenience of concept demonstration, porous zinc oxide (ZnO) nanosheets solid was selected as the self-sacrificial template and 2D nanostructure-directing agent to prepare 2D ZIF-8 derived carbon nanosheets (ZCNs). The as-prepared carbon nanosheets exhibit graphene-like morphology, large surface area with hierarchical porosity. ZCNs with these unique characterizations exhibits advanced performance as electrode materials for supercapacitors and Li-S batteries.

2. Results and Discussion

Our method to control the porous structure and dimension of ZIF-8 derived carbon material is based on the self-sacrificing template synthesis. As schematically presented in **Figure 1**a, porous ZnO nanosheets was used as the self-sacrificial template and 2D nanostructure-directing agent. Firstly, with the assistance of solvents and MeIm, Zn^{2+} was released from

This article is protected by copyright. All rights reserved

Author Manuscript

ZnO and then initiates the in situ growth of ZIF-8 on the surface of ZnO. ZIF-8@ZnO core–shell nanostructure was produced in this procedure. During the subsequent carbonization process, pyrolysis of ZIF-8 shell leaves microporous carbon wall. Simultaneously, carbothermal reduction of ZnO core and vaporization of Zn metal created dense mesopores, thus obtaining 2D carbon nanosheets with hierarchically porous nanostructure. In particular, the thickness of carbon wall and the size of mesopores could be adjusted by controlling the growth time of ZIF-8 shell. The ZIF-8 derived carbon nanosheets are denoted as ZCNs-*n*, where *n* represents the growth time of ZIF-8 (4 and 12 h).

To track the formation process of the hierarchical porous 2D carbon nanosheets, time-dependent reactions were carried out and the structures and morphologies of products were characterized. The successful preparation of ZnO@ZIF-8 precursor was firstly confirmed by powder X-ray diffraction (XRD). The XRD patterns reveal that ZnO@ZIF-8 precursors prepared with different reaction time are the composites of ZnO and ZIF-8 (Figure 1b). The main peaks and relative intensity agree well with those of ZnO and simulated ZIF-8. As highlighted in the right column, compared with ZnO template, the (101) peaks of ZnO in ZnO@ZIF-8 precursors are lower in intensity and wider in the full width at half maximum. These changes indicate that the content and size of ZnO nanoparticles decreased. Scanning electron microscopy (SEM) images display that the ZnO nanosheets are composed of inter-connected nanoparticles with size of 40–50 nm (Figure c, d). The thickness is approximately 15 nm. After growth for 4 h, the inter-particle pores were completely occupied by ZIF-8 and the nanosheets became thicker (Figure S1). With prolonged growth time to 12 h, the nanosheets became much thicker and tended to aggregate. In the SEM images, ZIF-8 polyhedrons were not observed, verifying the directed-growth of ZIF-8 along the surface of ZnO nanosheets. Transmission electron microscopy (TEM) and high-resolution TEM (HRTEM) images confirm the core–shell structure of ZnO@ZIF-8 (Figure 1e, f). ZnO

Author Manuscript

This article is protected by copyright. All rights reserved

nanoparticles were completely embedded in the ZIF-8 and the size of ZnO nanoparticles decreases to 10~15 nm. Moreover, the ZIF-8 was quite compact and no cracks were observed.

2D carbon nanosheets were obtained by direct pyrolysis of ZnO@ZIF-8 precursor without any chemical activation or template etching process. Thermogravimetric analyses (TGA) were performed to investigate the carbonization process (Figure S2). The first step is attributed to the pyrolysis of ZIF-8 between 500 to 600 °C, while the second step above 700 °C is indicative for the carbothermal reduction of ZnO.[4f,10] So the carbonization process was set at 950 °C and hold for 10 h, ensuring the completely reduction of ZnO and vaporization of Zn. XRD pattern and Raman spectra confirm that no ZnO or Zn metal impurities remained in the as-prepared carbon (Figure S3). In the XRD pattern, two broad peaks located at around 25° and 44° were assigned to the characteristic carbon (002) and (100) diffractions, respectively, revealing the presence of long-range 2D ordering in the carbon matrices along with some graphitization. The Raman spectra of ZCNs-4 present a D-band at 1359 cm^{-1} and a G-band at1602 cm^{-1}, which are related to defect and graphitization, respectively. The high value of I_D/I_G (1.07) of ZCNs-4 indicates high graphitization degree. In addition, the shapes of the D and 2D bands (at approximately 2765 cm^{-1}) show features of few-layered graphene.[3c,11] As revealed in SEM images (Figure S4), the as-prepared carbon materials show graphene-like morphology with abundant crumples and inter-connected macropores. We could observe that the carbon materials are composed of thin carbon nanosheets (Figure 1e, f). Moreover, it is worth mentioning that this synthesis method could also fabricate ZIF-8-derived carbon materials with other unique nanostructure. By using ZnO sphere, we could prepare zero-dimensional (0D) ZIF-8 derived hollow carbon sphere (Figure S5). On the whole, all these results support the self-sacrificial template-directed synthesis of ZIF-8 derived carbon materials with controllable dimension.

As shown in **Figure 2**a and b, TEM images clearly show that the 2D porous carbon nanosheets show hierarchically porous nanostructure, which is constituted by microporous

This article is protected by copyright. All rights reserved

Author Manuscript

wall and mesoporous hollow. It is noted that a highly porous structure with thin and unbroken carbon walls can be obtained. In addition, we could observe that the ZCNs-12 shows thicker carbon wall and are more compact. HRTEM image shows carbon walls of less than 5 nm in thickness and abundant disordered graphene layer in ZCNs-4 (Figure 2c). The formation of hierarchical porosity are attributed to two factors: (1) as widely reported in previous reports, carbonization of ZIF-8 will lead to highly microporous carbon;[3a,4b] (2) the reduction of ZnO nanoparticles by consumption of carbon atom and vaporization of Zn metal created dense mesopores in the interior of carbon nanosheets.[4a,10] STEM image further confirms hierarchically porous nanostructure distributed in the inter-connected thin carbon nanosheets.

Nitrogen adsorption experiment was further performed to examine the pore characteristics of the 2D carbons nanosheets. The N_2 sorption isotherms of ZCNs-4 and ZCNs-12 both exhibit characteristics of type I/IV (Figure 2e). The steep adsorption at low relative pressure indicates a high amount of micropores and the hysteresis loop at high relative pressure suggests the formation of mesoporous structure, confirming the hierarchically porous structure of ZCNs. The BET surface area (S_{BET}) of ZCNs-4 and ZCNs-12 are up to 1228 and 1023 $m^2\ g^{-1}$, respectively. Furthermore, notable feature of high ratio of meso/macropore volume to micropore volume ($V_{meso+macro}/V_{micro}$) was observed. For ZCNs-4 and ZCNs-12, the $V_{meso+macro}/V_{micro}$ ratios are up to 2.46 and 2.22, respectively, which are much higher than that of ZIF-8 derived carbon.[3b,4b,12] According to the non-local density functional theory (NLDFT) model, ZCNs-4 and ZCNs-12 show similar microporous distribution with maximum frequencies near 0.6 and 1.3 nm (Figure 2f). However, the mesopores in ZCNs-12 are smaller than ZCNs-4. This is because longer time growth of ZIF-8 shell leaves smaller ZnO core.

To evaluate the chemical identities of the heteroatoms in the ZCNs materials, X-ray photoelectron spectroscopy (XPS) and X-ray absorption near edge structure (XANES) measurements were carried out. The XPS confirmed that ZCNs-4 exhibits a predominant peak at 284.7 eV corresponding to C 1s, 531.4 eV to O 1s, and 399.5 eV to N 1s (Figure S6). The

This article is protected by copyright. All rights reserved

Author Manuscript

atomic concentration of N in ZCNs-4 is up to 4.64%. The high resolution C 1s spectrum of ZCNs-4 can be deconvoluted into three individual component peaks, corresponding to C=C sp^2 (284.6eV), C–C sp^3 (285.7eV) and C–O/C–N (286.6 eV) (**Figure 3**a).[4f] The ratio of C=C/C-C was up to 96%, indicating high graphitization degree. The N 1s spectrum (Figure3b) can be fitted by three peaks located at 400.8, 399.7 and 398.2 eV, which are attributed to quaternary (N-Q), pyrrolic (N-5), and pyridinic (N-6) nitrogen, respectively.[3c,4f] As shown in the C-K edge XANES, peaks C1and C2 at around 285 and 292.4 eV were due to C–C π* (ring) and C–C σ* (ring) transitions, respectively (Figure 3c).[13] The high intensity of C1 peak further confirms the high graphitization degree of ZCNs-4. The adsorptions in the 286–290 eV region correspond to carbon atoms that are attached to either oxygen or nitrogen atoms. In the N-K XANES spectra, three well resolved resonance peaks located at N1 (~397.9eV), N2 (~400.7eV), and N3 (~406.8eV), respectively, are observed. Peak N1 and N3 are attributed to the pyridinic (C=N π*) and graphitic type nitrogen species, respectively. Peak N2 is assigned to general transitions from the N 1s core level to C–N s* states.[13] The XPS and XANES results proved that the carbon materials prepared by this self-sacrificial template-directed synthesis show a high graphitization degree and high-level nitrogen doping.

The unique 2D nanostructure, high-level nitrogen doping, and expected large surface area with hierarchical porosity render ZCNs advanced electrode materials for supercapacitor, which showcase significant advantages of high power density and long cycling life.[6] **Figure 4** shows the electrochemical characterization results of ZCNs electrode in 6M KOH aqueous electrolyte with a symmetrical two-electrode system. Rectangular cyclic voltammetry (CV) curves of ZCNs-4 were presented in Figure 4a. It can be seen that the CV curves display a nearly rectangular shape even at 200 mV s^{-1}, highlighting the typical supercapacitive behaviors. The galvanostatic charge/discharge curves of ZCNs-4 at different current densities exhibit a symmetric triangle feature without obvious potential drop, (Figure 4b), further

This article is protected by copyright. All rights reserved

Author Manuscript

indicting very efficient charge transfer within the ZCNs-4 electrode. Figure 4c compares the calculated specific capacitances of the ZCNs-4 and ZCNs-12 electrodes at different current densities. At a current density of 0.5 A g^{-1}, the specific capacitances of ZCNs-4 and ZCNs-12 are up to 220 and 208 F g^{-1}, respectively. The high specific capacitances may be attributed to the large ion-accessible surface area for forming electrical double layer and pseudocapacitive contribution of the nitrogen-containing functional groups.[4b,14] With increasing current density, ZCNs-4 electrode manifests higher specific capacitance than ZCNs-12. At 20 A g^{-1}, ZCNs-4 still exhibit a specific capacitance of 177 F g^{-1}, exhibiting excellent rate capability.

Supercapacitive performance of ZCNs-4 was further analyzed by electrochemical impedance spectroscopy (EIS) technique. ZCNs-4 obviously shows smaller charge transfer resistance and ion transport resistance (Figure S7a). In addition, ZCNs-4 device shows smaller time constant τ_0 of (1.28 s) than that of ZCNs-12 electrode (2.94 s) (Figure S7b). The lower time constant clearly demonstrates the crucial role of thinner carbon wall in greatly promoting the ion kinetics in the interior of the electrodes. Significantly, in term of specific capacitance and rate capability, the ZCNs-4 shows greatly improved performances than of ZIF-8 microcrystal-derived carbon materials and are comparable with other advanced 2D carbon materials.[12,15] All these results indicate that ZCNs-4 shows greatly improved performances, which could be attributed to its unique 2D porous nanostructure and high-level nitrogen doping. This nanostructure not only ensures the fast ion diffusion by shortening the diffusion pathways, but also provides continuous electron pathways. In addition, the nitrogen doping improves the electrical conductivity and wettability, and thus further enhances the ion transfer efficiency. ZCNs-4 with higher $V_{meso+macro}/V_{micro}$ volume ratio and thinner nanosheets structures offers faster ion transport channels, resulting in the higher capacitance retention at high current density. Furthermore, ZCNs-4 also exhibits excellent cycling performance, possessing a high capacitance retention over 97% after 5000 galvanostatic charge/discharge cycles at 2 A g^{-1} (Figure 4d).

This article is protected by copyright. All rights reserved

Author Manuscript

The large surface area, unique 2D nanostructure with microporous wall and mesoporous hollow, high level nitrogen doping also make ZCNs as advanced sulfur immobilizers for Li–S batteries, which showcase significant advantages of high energy density (1600 Wh kg^{-1}) and low cost.[16] As shown in SEM image (**Figure 5**a), the encapsulation sulfur into the ZCNs-4 induced no obvious changes in morphology. No bulk sulfur particles or aggregations were detected on the external surface of the ZCNs-4. The TEM images in Figure 5b indicate that the sulfur is homogeneously dispersed in the porous carbon matrix. STEM image and corresponding element mapping also indicated the homogeneous dispersion of sulfur in the ZCNs-4 matrix (Figure5c). Raman spectra further confirm good distribution of incorporated sulfur (Figure S8). The absence of peak of sulfur indicates that sulfur is confined in the pores and shows amorphous structure. The intimate contact between the sulfur and graphene layers is critical for rapid electron transport. A sulfur loading of ca. 60 wt% was determined by TGA (Figure S9). Meanwhile, two steps in the sulfur evaporation process are observed for ZCNs-4/S composite, indicating that elemental sulfur is incorporated not only in the microporous carbon wall but also in the internal mesopores.[17]

The CV profile of ZCNs-4/S electrode shows three peaks in the cathodic scan and one peak in the anodic scan (Figure S10). According to the reported mechanisms for the reduction and oxidation of sulfur during the charge/discharge process, the first peak at 2.4 V corresponds to the reduction of elemental sulfur to long-chain lithium polysulfides (Li_2S_n, $4 \leq n \leq 8$). The second peak at 2.04 V corresponds to the further reduction of the long-chain lithium polysulfides to Li_2S_2/Li_2S. The reduction peak below 1.7 V corresponds to the reduction of small sulfur molecule (from $S_{2\sim4}$ to Li_2S_2/Li_2S), which was confined in the microporous carbon wall. The oxidation peak at 2.33V is attributed to the conversion of Li_2S_2/Li_2S to polysulfides.[18] At a current density of 0.5 C, after one cycle of activation, the ZCNs-4/S electrode shows a specific capacity of 931 mAh g^{-1} at the 2nd cycle (**Figure 6**a). After cycling for 100 cycles, ZCNs-4/S electrode still derivers a specific capacity of 663 mAh

This article is protected by copyright. All rights reserved

Author Manuscript

g^{-1}. At a current density of 1 C, after 200 cycles, the specific capacity is up to 450 mAh g^{-1}, exhibiting that 2D porous host suspend the dissolution of lithium polysulfides during charge/discharge process (Figure 6b). Comparatively, the ZCNs-12/S electrode shows lower specific capacity and poorer cycling performance. ZCNs-12/S electrode only derivers a specific capacity of 412 mAh g^{-1} after 100 cycles (Figure S11a, b). This may be due to the low surface area and more compact structure of ZCNs-12. To further investigate the roles of 2D porous carbon, capacity contributions from three discharge plateaus were distinguished from the potential profiles of ZCNs-4/S electrode (Figure S11c, d). The extent of dissolution of polysulfides could lead to the decay of capacity contribution from the upper discharge plateau.[19] The capacity retention of the upper plateau of the ZCNs-4/S composite was 70% after 100 cycles at 0.5 C. The high capacity retention can be attributed to the unbroken microporous carbon wall and lithium polysulfide binding capability of the nitrogen functional groups, suppressing the dissolution and shuttle of polysulfides.[20] This method provide a new possibility to prepare advanced sulfur immobilizer for long-term Li-S batteries.

3. Conclusion

A self-sacrificial template-directed synthesis method was developed for controlling the porous structure and dimension of ZIF-8-derived carbon materials. By using porous ZnO nanosheets as the self-sacrificial template and 2D nanostructure-directing agent, 2D ZIF-8 derived carbon nanosheets could be obtained by direct pyrolysis of core–shell nanostructured ZnO@ZIF-8 precursor. The as-prepared 2D ZCNs materials exhibit high graphitization degree, large surface area, and unique hierarchical porosity, showing promising potential for electrochemical energy-storage devices. When used as the electrode for supercapacitors, ZCNs-4 electrode exhibits an outstanding specific capacity of 220 F g^{-1} at 0.5 A g^{-1}, and still remain 177 F g^{-1} at 20 A g^{-1}. Meanwhile, the unique properties make ZCNs advanced sulfur immobilizer for improving the electron/ion transport and suppressing the dissolution and shuttle of polysulfides. We believe that the 0D and 2D nanostructures, achieved by using

This article is protected by copyright. All rights reserved

Author Manuscript

porous ZnO sphere and ZnO nanosheets, can be extended to other nanostructures by using other templates, such as ZnO film, ZnO nanowires array and cobalt oxide nanowires array. This versatile synthetic method enables MOF-derived porous carbon to exploit its full potential in energy-storage applications.

4. Experimental Section

Synthesis of ZCNs materials. In a typical synthesis, 204 mg ZnO nanosheets was added to 80 mL N,N-dimethylformamide/H_2O mixed solvent (v/v ratio of 3:1) and stirred for 1 h. Then 206 mg 2-methylimidazole (MeIM) was added to the dispersion under magnetic stirring. After stirring for 5 min, the homogeneous dispersion was added to Teflon-lined stainless-steel autoclave (100 mL). The autoclave was transferred to an oven. After the mixture reacted for 4 and 12 h at 70 °C, the white product was collected by centrifugation and washed by fresh DMF and ethanol for five times. The as-prepared ZnO@ZIF-8 composite was put into a crucible and transferred into a temperature-programmed furnace, then heated to 200 °C for 6 h at a heating rate of 5 °C min^{-1}. The further pyrolysis treatment was performed at 950 °C for 10 h at a heating rate of 2 °C min^{-1}.

Preparation of ZCNs-4/S composite. The ZCNs-4/S composite was prepared through a melt-diffusion strategy. Typically, ZCNs-4 and elemental sulfur were mixed together and placed in a crucible, and then the mixture was heated to 155 °C and kept at the temperature for 20 h.

Characterization. X-ray diffraction (XRD) was studied by Bruker D8 Advance X-ray diffractometer using Cu Kα radiation. The morphologies were characterized by scanning electron microscope (Hitachi 4800) and transmission electron microscopy (Tecnai G2 F20). Raman spectra were conducted on the HORIBA Scientific LabRAM HR Raman spectrometer system with a 532.4 nm laser. Thermogravimetric analysis was conducted on a TG-DSC instrument (NETZSCH STA 409 PC) under nitrogen protection. The X-ray photoelectron spectroscopy analysis was performed on a Perkin-Elmer PHI 550 spectrometer with Al Kα

This article is protected by copyright. All rights reserved

Author Manuscript

(1486.6 eV) as the X-ray source. X-ray absorption near edge structure (XANES) at the C K-edge and N K-edge were collected on the beamline 08U at the Shanghai Synchrotron Radiation Facility (SSRF). The N_2 adsorption-desorption isotherms of the samples were conducted by a Micromeritics BK122T-Banalyzer. The specific surface area was calculated using the Brunauer–Emmett–Teller method. The total pore volume and pore size distribution were obtained from non-local density functional theory (NLDFT) model.

Cell fabrication and measurements for supercapacitors. The supercapacitor performances were carried out by a symmetric sandwich-type two-electrode system in 6 M KOH electrolyte. The electrodes were prepared by pressing a slurry of porous carbon nanosheets, carbon black and polytetrafluoroethylene (PTFE) in the ratio of 80:15:5 onto a nickel foam current collector (1×1 cm^2) and then dried at 110 ºC for 12 h. The active material mass loading for each electrode is about 2.5 mg cm^{-2}. A sandwich-type supercapacitor consisting of two similar sample electrodes was assembled. The cyclic voltammetry (CV), galvanostatic charge/discharge, and electrochemical impedance spectroscopy (EIS) tests were executed using a CHI 660E electrochemical workstation. EIS was conducted at in the frequency range of 10^5 Hz to 10^{-2} Hz with the amplitude of 5 mV. Galvanostatical charge/discharge cycling was performed on a CT2001A cell test instrument (LAND Electronic Co.) The gravimetric capacitance(C) was calculated based on the following equation, $C = (4I\Delta t)/(m\Delta V)$, where I is the constant discharge current, Δt is the discharge time, m is the total mass of two electrode materials and ΔV represents voltage range (excluding the IR drop).

Cell fabrication and measurements for Li–S batteries. The ZCNs-4/S electrodes were prepared at a slurry coating procedure. The slurry consisted of ZCNs-4/S composite, acetylene black and polyvinylidene fluoride (PVDF) at a weight ratio of 70:20:10 in N-methyl pyrrolidinone, and was uniformly spread on an aluminium foil current collector and then was dried at 60 °C for 12 h. The active material loading was in the range of 0.6~0.8 mg cm^{-2}.

This article is protected by copyright. All rights reserved

Author Manuscript

CR2016-type coin cell cells were assembled in an argon-filled glove box. Lithium foil was used as the counter electrode and the separator was Celgard 2400. The electrolyte was composed of 1 M Bis-(trifluoromethane) sulfonimide lithium (LiTFSI) salt and 0.1 M $LiNO_3$ additive dissolved in a mixed solvent of 1,3-dioxolane (DOL) and 1,2-dimethoxyethane (DME) (1:1 by volume). CV was performed on a CHI 660E electrochemical workstation. Galvanostatic charge/discharge cycling was performed on a CT2001A cell test instrument (LAND Electronic Co.).

Supporting Information
Supporting Information is available from the Wiley Online Library or from the author.

Acknowledgements
The work was funded by the National Key Basic Research Program 973 (No. 2014CB239701), NSFC (No. 21173120, No. 51372116), Natural Science Foundation of Jiangsu Province (No. BK2011030, No. BK20151468), Fundamental Research Funds for the Central Universities of NUAA (NP2014403) and Priority Academic Program Development of Jiangsu Higher Education Institutions (PAPD). B. Ding is grateful to Funding of Jiangsu Innovation Program for Graduate Education (CXZZ13_0158), Outstanding Doctoral Dissertation in NUAA (BCXJ13-13) and the Fundation of Graduate Innovation Center in NUAA (kfjj130219).

Received: ((will be filled in by the editorial staff))
Revised: ((will be filled in by the editorial staff))
Published online: ((will be filled in by the editorial staff))

[1] a) P. Simon, Y. Gogotsi, *Acc. Chem. Res.* **2012**, *46*, 1094; b) F. Bonaccorso, L. Colombo, G. Yu, M. Stoller, V. Tozzini, A. C. Ferrari, R. S. Ruoff, V. Pellegrini, *Science* **2015**, *347*.

[2] a) S. L. Candelaria, Y. Shao, W. Zhou, X. Li, J. Xiao, J.-G. Zhang, Y. Wang, J. Liu, J. Li, G. Cao, *Nano Energy* **2012**, *1*, 195; b) L. Hao, X. Li, L. Zhi, *Adv. Mater.* **2013**, *25*, 3899; c) Y. Zhu, S. Murali, M. D. Stoller, K. J. Ganesh, W. Cai, P. J. Ferreira, A. Pirkle, R. M. Wallace, K. A. Cychosz, M. Thommes, D. Su, E. A. Stach, R. S. Ruoff, *Science* **2011**, *332*, 1537; d) X. L. Ji, K. T. Lee, L. F. Nazar, *Nat. Mater.* **2009**, *8*, 500; e) Q. Sun, B. He, X.-Q. Zhang, A.-H. Lu, *ACS Nano* **2015**, *9*, 8504; f) J. T. Lee, Y. Zhao, S. Thieme, H. Kim, M.

This article is protected by copyright. All rights reserved

Author Manuscript

Oschatz, L. Borchardt, A. Magasinski, W.-I. Cho, S. Kaskel, G. Yushin, *Adv. Mater.* **2013**, *25*, 4573.

[3] a) J.-K. Sun, Q. Xu, *Energy Environ. Sci.* **2014**, *7*, 2071; b) J. Tang, R. R. Salunkhe, J. Liu, N. L. Torad, M. Imura, S. Furukawa, Y. Yamauchi, *J. Am. Chem. Soc.* **2015**, *137*, 1572; c) F. Zheng, Y. Yang, Q. Chen, *Nat. Commun.* **2014**, *5*, 5261.

[4] a) S. J. Yang, T. Kim, J. H. Im, Y. S. Kim, K. Lee, H. Jung, C. R. Park, *Chem. Mater.* **2012**, *24*, 464; b) W. Chaikittisilp, M. Hu, H. Wang, H. S. Huang, T. Fujita, K. C. Wu, L. C. Chen, Y. Yamauchi, K. Ariga, *Chem. Commun.* **2012**, *48*, 7259; c) S. Lim, K. Suh, Y. Kim, M. Yoon, H. Park, D. N. Dybtsev, K. Kim, *Chem. Commun.* **2012**, *48*, 7447; d) N. L. Torad, M. Hu, Y. Kamachi, K. Takai, M. Imura, M. Naito, Y. Yamauchi, *Chem. Commun.* **2013**, *49*, 2521; e) J.-W. Jeon, R. Sharma, P. Meduri, B. W. Arey, H. T. Schaef, J. L. Lutkenhaus, J. P. Lemmon, P. K. Thallapally, M. I. Nandasiri, B. P. McGrail, S. K. Nune, *ACS Appl. Mater. Interfaces* **2014**, *6*, 7214; f) L. Zhang, Z. Su, F. Jiang, L. Yang, J. Qian, Y. Zhou, W. Li, M. Hong, *Nanoscale* **2014**, *6*, 6590; g) K. Xi, S. Cao, X. Peng, C. Ducati, R. V. Kumar, A. K. Cheetham, *Chem. Commun.* **2013**, *49*, 2192; h) H. B. Wu, S. Wei, L. Zhang, R. Xu, H. H. Hng, X. W. Lou, *Chem. Eur. J.* **2013**, *19*, 10804; i) G. Y. Xu, B. Ding, L. F. Shen, P. Nie, J. P. Han, X. G. Zhang, *J. Mater. Chem. A* **2013**, *1*, 4490.

[5] a) S. Dutta, A. Bhaumik, K. C. W. Wu, *Energy Environ. Sci.* **2014**, *7*, 3574; b) D. W. Wang, F. Li, M. Liu, G. Q. Lu, H. M. Cheng, *Angew. Chem. Int. Ed.* **2008**, *120*, 379; c) M. Oschatz, L. Borchardt, K. Pinkert, S. Thieme, M. R. Lohe, C. Hoffmann, M. Benusch, F. M. Wisser, C. Ziegler, L. Giebeler, M. H. Ruemmeli, J. Eckert, A. Eychmueller, S. Kaskel, *Adv. Energy Mater.* **2014**, *4*, 1300645; d) T. Kim, G. Jung, S. Yoo, K. S. Suh, R. S. Ruoff, *ACS Nano* **2013**, *7*, 6899.

[6] a) X. Zheng, J. Luo, W. Lv, D. W. Wang, Q. H. Yang, *Adv. Mater.* **2015**, *27*, 5388; b) L. Dai, D. W. Chang, J.-B. Baek, W. Lu, *Small* **2012**, *8*, 1130.

This article is protected by copyright. All rights reserved

Author Manuscript

[7] a) H. Wang, Z. Xu, A. Kohandehghan, Z. Li, K. Cui, X. Tan, T. J. Stephenson, C. K. King'ondu, C. M. Holt, B. C. Olsen, *ACS Nano* **2013**, *7*, 5131; b) X. Yang, L. Zhang, F. Zhang, Y. Huang, Y. Chen, *ACS Nano* **2014**, *8*, 5208; c) M. Q. Zhao, Q. Zhang, J. Q. Huang, G. L. Tian, J. Q. Nie, H. J. Peng, F. Wei, *Nat. Commun.* **2014**, *5*, 3410.

[8] a) A. D. Roberts, X. Li, H. Zhang, *Chem. Soc. Rev.* **2014**, *43*, 4341; b) H. J. Lee, S. Choi, M. Oh, *Chem. Commun.* **2014**, *50*, 4492; c) H. X. Zhong, J. Wang, Y. W. Zhang, W. L. Xu, W. Xing, D. Xu, Y. F. Zhang, X. B. Zhang, *Angew. Chem. Int. Ed.* **2014**, *53*, 14235; d) J.-K. Sun, Q. Xu, *Chem. Commun.* **2014**, *50*, 13502.

[9] a) Y.-L. Ding, J. Xie, G.-S. Cao, T.-J. Zhu, H.-M. Yu, X.-B. Zhao, *Adv. Funct. Mater* **2011**, *21*, 348; b) F. Zou, X. Hu, Z. Li, L. Qie, C. Hu, R. Zeng, Y. Jiang, Y. Huang, *Adv. Mater.* **2014**, *26*, 6622; c) E. Zanchetta, L. Malfatti, R. Ricco, M. J. Styles, F. Lisi, C. J. Coghlan, C. J. Doonan, A. J. Hill, G. Brusatin, P. Falcaro, *Chem. Mater.* **2014**, *27*, 690; d) W. W. Zhan, Q. Kuang, J. Z. Zhou, X. J. Kong, Z. X. Xie, L. S. Zheng, *J. Am. Chem. Soc.* **2013**, *135*, 1926.

[10] P. Strubel, S. Thieme, T. Biemelt, A. Helmer, M. Oschatz, J. Brückner, H. Althues, S. Kaskel, *Adv. Funct. Mater.* **2015**, *25*, 287.

[11] A. C. Ferrari, D. M. Basko, *Nat. Nanotech.* **2013**, *8*, 235.

[12] A. J. Amali, J. K. Sun, Q. Xu, *Chem. Commun.* **2014**, *50*, 1519.

[13] a) L.-S. Zhang, X.-Q. Liang, W.-G. Song, Z.-Y. Wu, *Phys. Chem. Chem. Phys.* **2010**, *12*, 12055; b) J. Zhong, J.-J. Deng, B.-H. Mao, T. Xie, X.-H. Sun, Z.-G. Mou, C.-H. Hong, P. Yang, S.-D. Wang, *Carbon* **2012**, *50*, 335.

[14] Z. Li, Z. Xu, X. Tan, H. Wang, C. M. B. Holt, T. Stephenson, B. C. Olsen, D. Mitlin, *Energy Environ. Sci.* **2013**, *6*, 871.

[15] H. Wang, L. Zhi, K. Liu, L. Dang, Z. Liu, Z. Lei, C. Yu, J. Qiu, *Adv. Funct. Mater.* **2015**, *25*, 5420.

This article is protected by copyright. All rights reserved

Author Manuscript

[16] a) A. Manthiram, Y. Z. Fu, Y. S. Su, *Acc. Chem. Res.* **2013**, *46*, 1125; b) Y. Yang, G. Zheng, Y. Cui, *Chem. Soc. Rev.* **2013**, *42*, 3018; c) L. Xiao, Y. Cao, J. Xiao, B. Schwenzer, M. H. Engelhard, L. V. Saraf, Z. Nie, G. J. Exarhos, J. Liu, *Adv. Mater.* **2012**, *24*, 1176; d) C. Wu, L. Fu, J. Maier, Y. Yu, *J. Mater. Chem. A* **2015**, *3*, 9438.

[17] a) C. D. Liang, N. J. Dudney, J. Y. Howe, *Chem. Mater.* **2009**, *21*, 4724; b) J. Guo, Y. Xu, C. Wang, *Nano Lett.* **2011**, *11*, 4288; c) L. Zeng, F. Pan, W. Li, Y. Jiang, X. Zhong, Y. Yu, *Nanoscale* **2014**, *6*, 9579.

[18] a) Z. Li, Y. Jiang, L. Yuan, Z. Yi, C. Wu, Y. Liu, P. Strasser, Y. Huang, *ACS Nano* **2014**, *8*, 9295; b) S. Xin, L. Gu, N. H. Zhao, Y. X. Yin, L. J. Zhou, Y. G. Guo, L. J. Wan, *J. Am. Chem. Soc.* **2012**, *134*, 18510.

[19] a) N. Jayaprakash, J. Shen, S. S. Moganty, A. Corona, L. A. Archer, *Angew. Chem. Int. Ed.* **2011**, *50*, 5904; b) G. Zhou, L.-C. Yin, D.-W. Wang, L. Li, S. Pei, I. R. Gentle, F. Li, H.-M. Cheng, *ACS Nano* **2013**, *7*, 5367; c) W. Kong, L. Sun, Y. Wu, K. Jiang, Q. Li, J. Wang, S. Fan, *Carbon* **2016**, *96*, 1053.

[20] a) J. Song, T. Xu, M. L. Gordin, P. Zhu, D. Lv, Y.-B. Jiang, Y. Chen, Y. Duan, D. Wang, *Adv. Funct. Mater.* **2014**, *24*, 1243; b) Y. Qiu, W. Li, W. Zhao, G. Li, Y. Hou, M. Liu, L. Zhou, F. Ye, H. Li, Z. Wei, S. Yang, W. Duan, Y. Ye, J. Guo, Y. Zhang, *Nano Lett.* **2014**, *14*, 4821.

Author Manuscript

This article is protected by copyright. All rights reserved

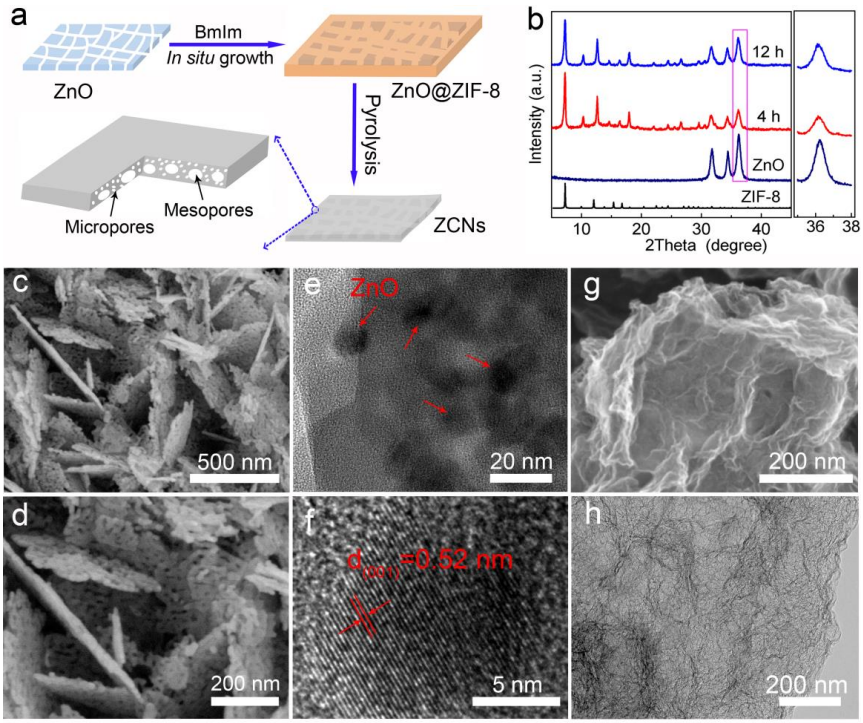

Figure 1. (a) Schematic illustration of self-sacrificial template-directed synthesis of ZCNs, where ZnO act as both Zn^{2+} resource for initial growth of ZIF-8 and self-sacrificial template for formation of mesopores. ZCNs show porous structure combined with microspores and mesopores. (b) XRD patterns of ZnO nanosheets and ZnO@ZIF-8 composites, the peaks corresponding to ZnO (101) reflections are highlighted in the right column. (c, d) SEM images of ZnO nanosheets template. (e) TEM and (f) HRTEM images of ZnO@ZIF-8 composite. (g) SEM image and (h) TEM image of ZCNs-4.

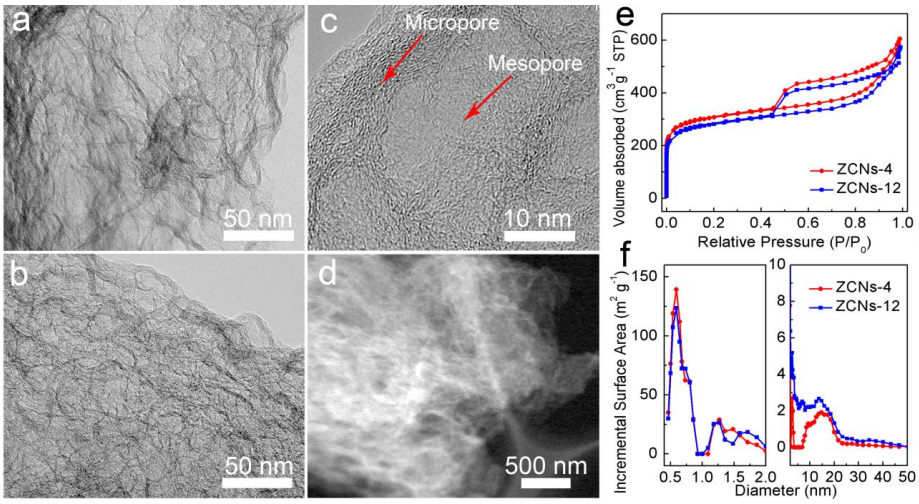

Figure 2. Structural and porous characterizations of ZCNs-4 and ZCNs-12: TEM images of (a) ZCNs-4 and (b) ZCNs-12. (c) HRTEM image and (d) STEM image of ZCNs-4. (e) N_2 sorption isotherms and (f) corresponding pore size distribution curves of ZCNs-4 and ZCNs-12.

This article is protected by copyright. All rights reserved

Author Manuscript

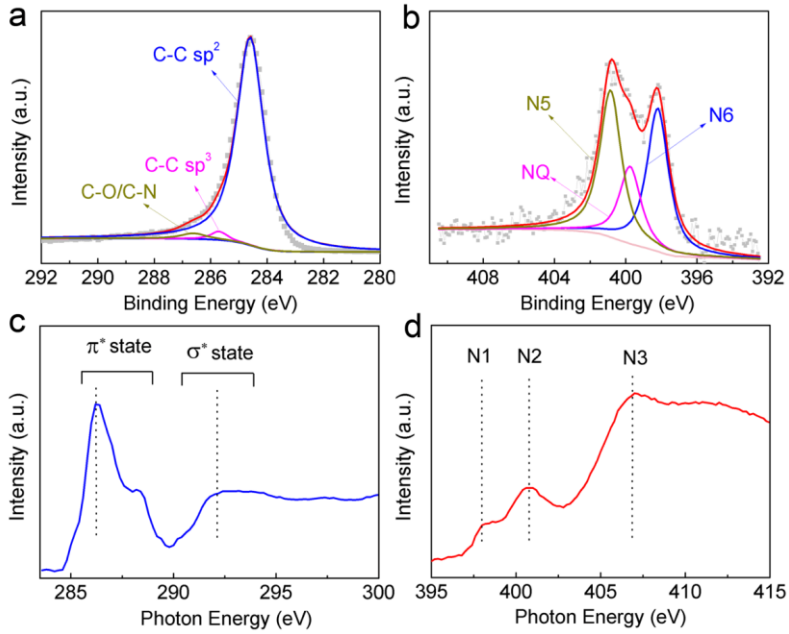

Figure 3. (a) High resolution C 1s and (b) N 1s XPS spectra of ZCNs-4. (c) C-K edge and (d) N-K edge XANES spectra of ZCNs-4.

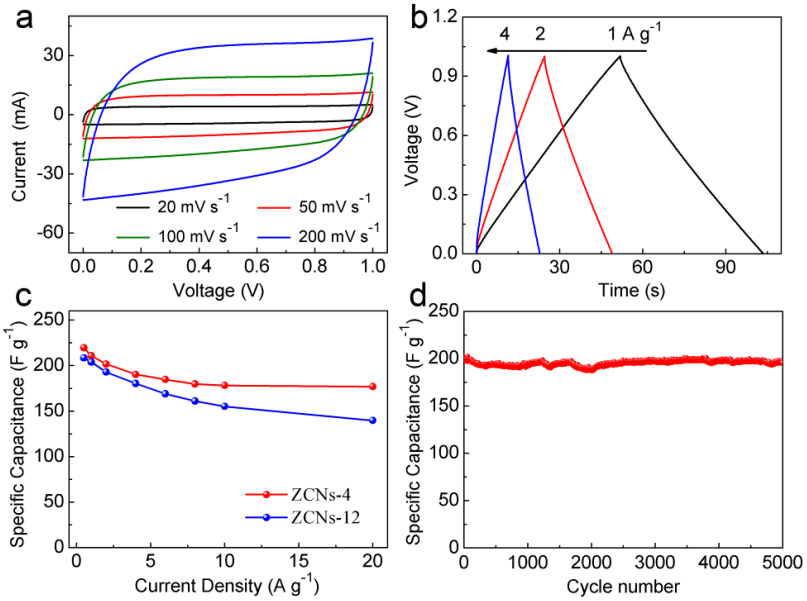

Figure 4. Electrochemical performance of ZCNs electrodes: (a) CV curves of ZCNs-4 at various scanning rates. (b) Galvanostatic charge/discharge curves under various current densities for ZCNs-4. (c) Specific capacitance dependence on current density of ZCNs-4 and ZCNs-12. (d) Long-term cycle stability of ZCNs-4 at current density of 2 A g^{-1}.

Author Manuscript

This article is protected by copyright. All rights reserved

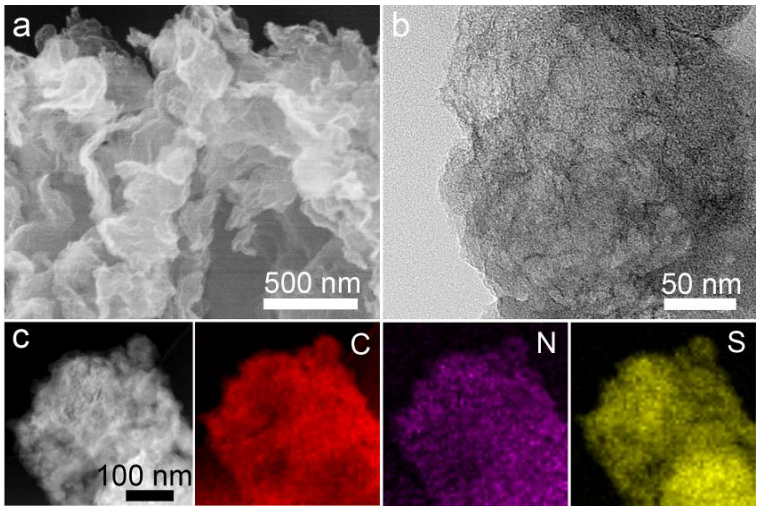

Figure 5. Structural characterizations of ZCNs-4/S composite: (a) SEM images. (b) TEM images. (c) STEM image and corresponding elemental mapping.

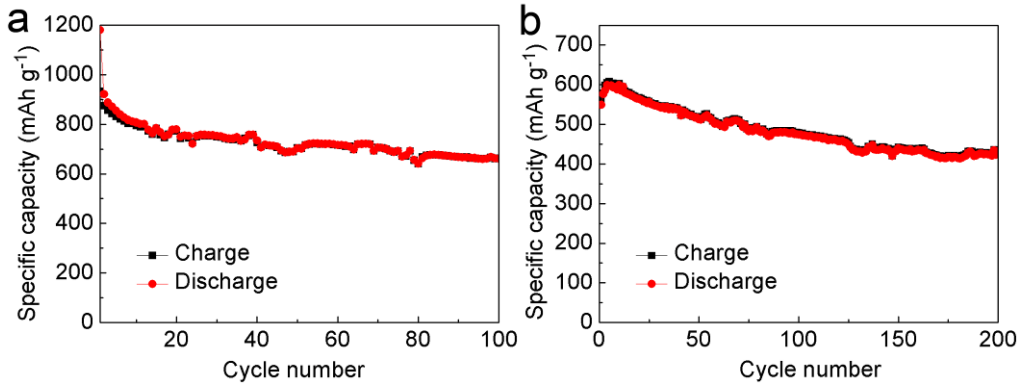

Figure 6. Cycling performance of ZCNs-4/S electrodes at (a) 0.5 and (b) 1 C.

Author Manuscript

This article is protected by copyright. All rights reserved

A self-sacrificial template-directed synthesis method is proposed to engineer the porosity and dimension of MOF-derived carbon materials. By using porous nanosheets solid as the self-sacrificial template and two-dimensional (2D) nanostructure-directing agent, 2D ZIF-8 derived carbon nanosheets are prepared, which exhibit large ion-accessible surface area and rapid ion transport as the electrode materials for electrochemical energy-storage devices.

Keyword: two-dimensional carbon, hierarchical porosity, metal–organic frameworks, self-sacrificial template, electrochemistry

B. Ding, J. Wang, Z. Chang, G. Y. Xu, X. D. Hao, Dr. L. F. Shen, Prof. H. Dou, Prof. X. G. Zhang

Self-Sacrificial Template-Directed Synthesis of Metal–Organic Framework-Derived Porous Carbon for Energy-Storage Devices

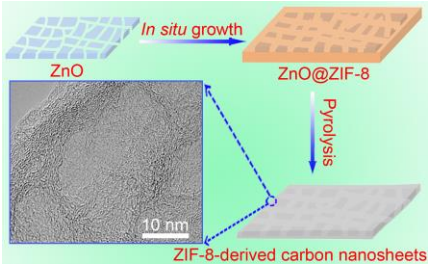

Author Manuscript

This article is protected by copyright. All rights reserved

Copyright WILEY-VCH Verlag GmbH & Co. KGaA, 69469 Weinheim, Germany, 2013.

Supporting Information

Self-sacrificial template-directed synthesis of metal–organic framework-derived porous carbon for energy-storage devicesitle

*Bing Ding, Jie Wang, Zhi Chang, Guiyin Xu, Xiaodong Hao, Laifa Shen, Hui Dou, Xiaogang Zhang**

Author Manuscript

Experiment Sections

Preparation of ZnO spheres. ZnO spheres were synthesized through hydrolysis of zinc acetate dihydrate in diethylene glycol as described in previous report.[S1] Typically, 1.97 g of zinc acetate dihydrate was added in 90 mL of diethylene glycol. The mixture was heated to 160 ºC at a rapid heating of about 10 ºC min^{-1} and then reflux at this temperature for 16 h. The product was collected by centrifuged and washed by ethanol several times. Then the white product was annealed at 400 °C for 1 h in air.

Preparation of hollow ZIF-8 derived carbon sphere. 204 mg ZnO nanosheets was added to 80 mL N,N-dimethylformamide/H_2O mixed solvent (v/v ratio of 3:1) and stirred for 1 h. Then 206 mg 2-methylimidazole (MeIM) was added to the dispersion under magnetic stirring. After 10 min stirring, the homogeneous dispersion was added to Teflon-lined stainless-steel autoclave (100 mL). The autoclave was transferred to an oven preheated to 70 °C. After the mixture reacted for 12 h, the white product was collected by centrifugation and washed by fresh DMF and ethanol for five times. The as-prepared ZnO@ZIF-8 composite was put into a ceramic boat and transferred into a temperature-programmed furnace, then heated to 200 °C for 6 h at a heating rate of 5 °C min^{-1}. The further pyrolysis treatment was performed at 950 °C for 10 h.

This article is protected by copyright. All rights reserved

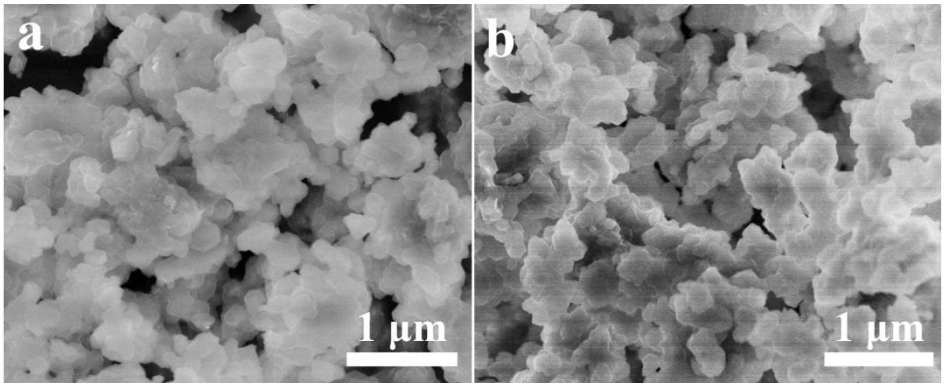

Figure S1. SEM images of ZnO@ZIF-8 composites prepared with (a) 4 h and (b) 12 h.

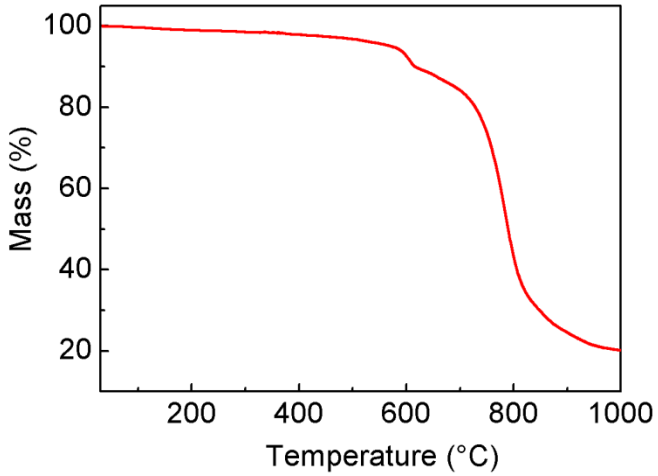

Figure S2. TGA curve of ZnO@ZIF-8 composite under N_2 conditions at a heating rate of 5 °C min^{-1} (ZnO@ZIF-8 composite was prepared at 4 h).

Author Manuscript

This article is protected by copyright. All rights reserved

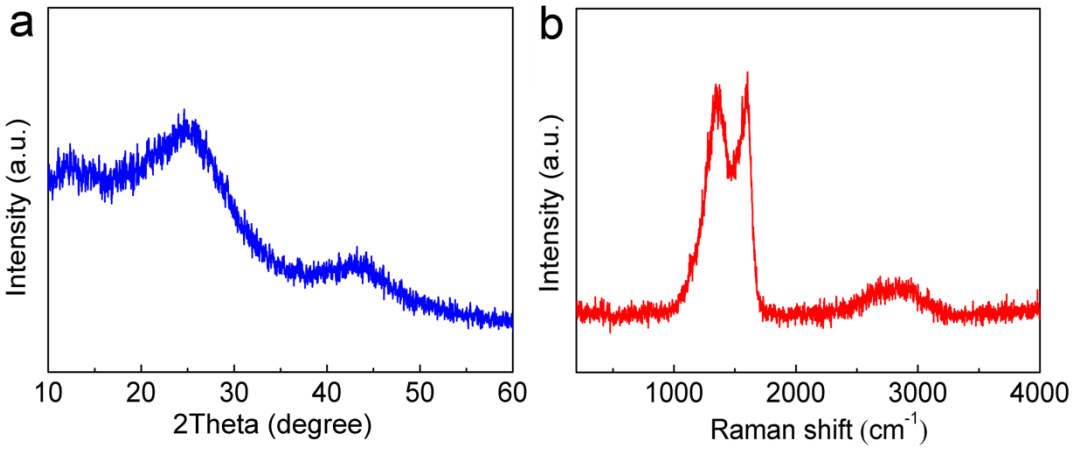

Figure S3. (a) XRD pattern and (b) Raman spectrum of ZCNs-4.

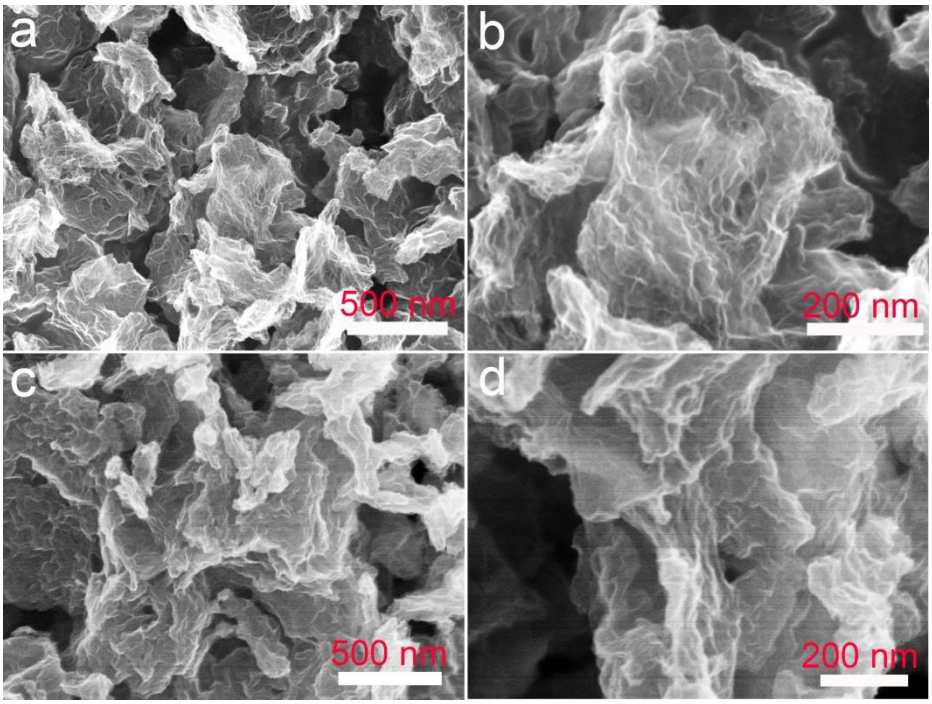

Figure S4. SEM images of (a, b) ZCNs-4 and (c, d) ZCNs-12.

Author Manuscript

This article is protected by copyright. All rights reserved

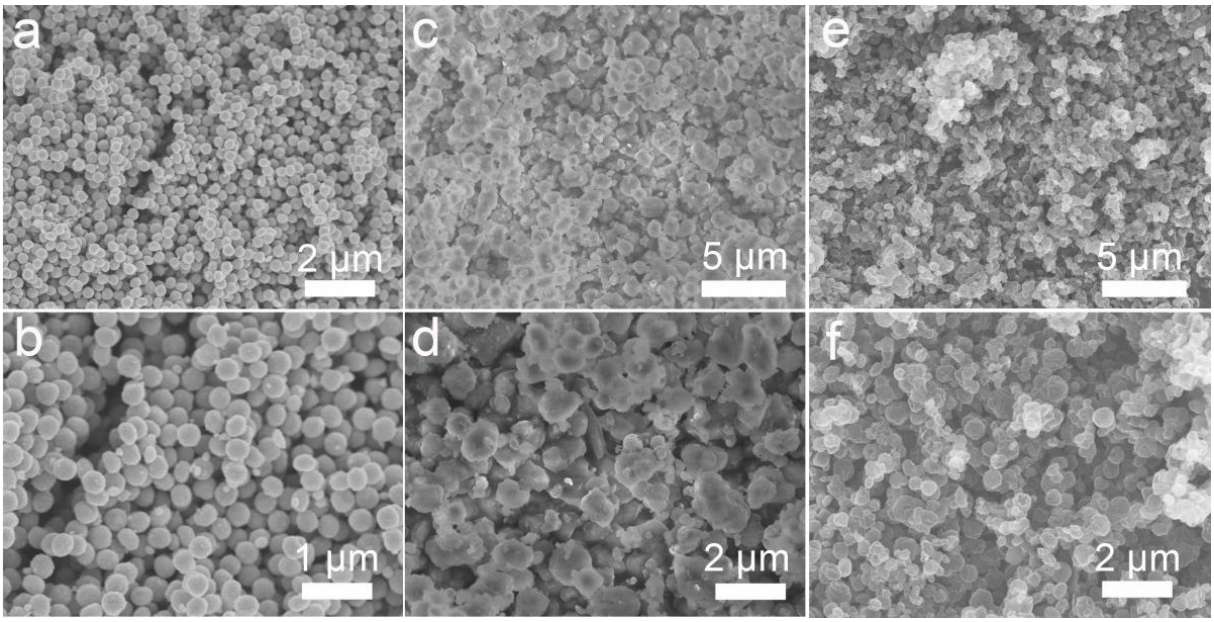

Figure S5. SEM images of (a, b) ZnO sphere, (c, d) core-shell nanostructured ZnO@ZIF-8 composite and (e, f) ZIF-8-derived hollow carbon sphere.

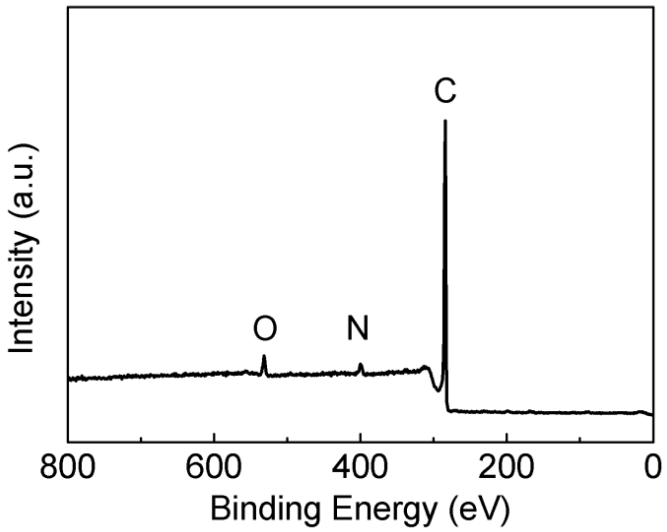

Figure S6. Typical survey scanned XPS spectrum of ZCNs-4.

Author Manuscript

This article is protected by copyright. All rights reserved

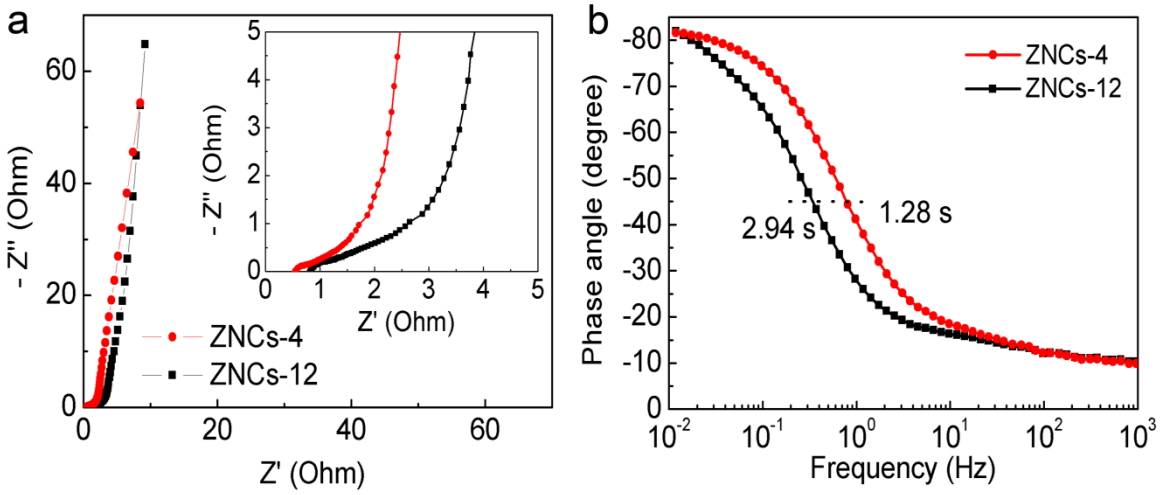

Figure S7. (a) Nyquist plots and (b) bode plots of ZCNs-4 and ZCNs-12-based cell.

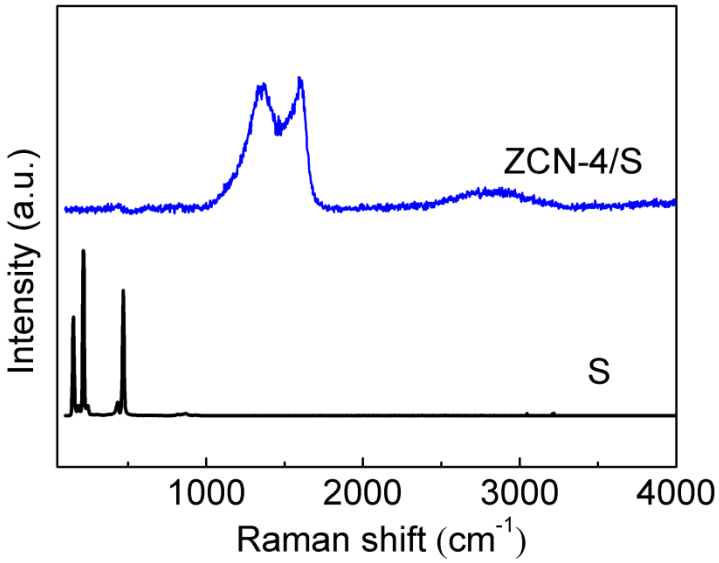

Figure S8. Raman spectra of elemental sulfur and ZCNs-4/S composite.

Author Manuscript

This article is protected by copyright. All rights reserved

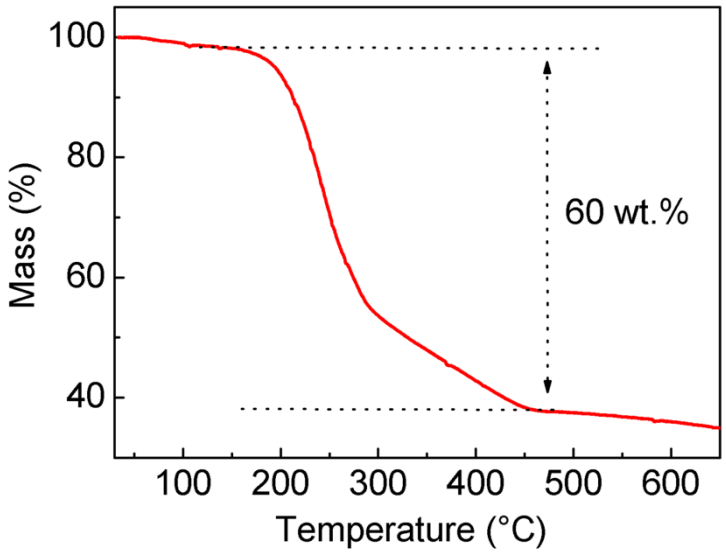

Figure S9. TG curves of elemental sulfur and ZCNs-4/S composite.

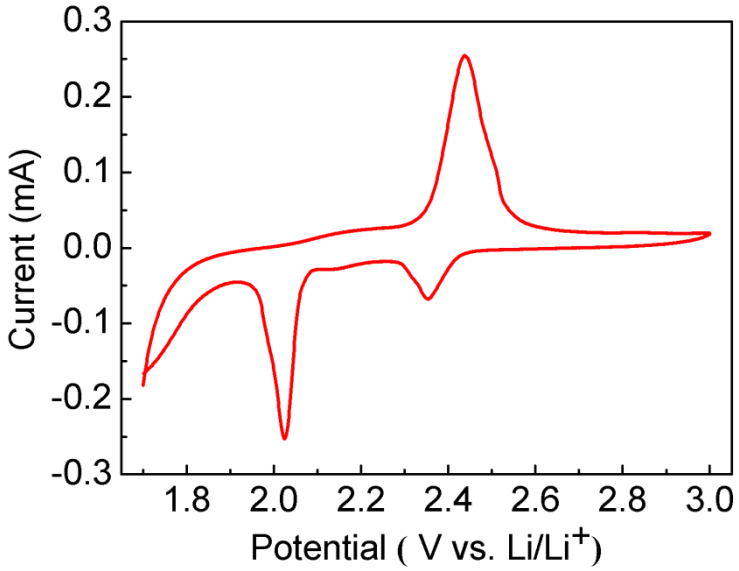

Figure S10. CV curve of ZCNs-4/S electrode.

Author Manuscript

This article is protected by copyright. All rights reserved

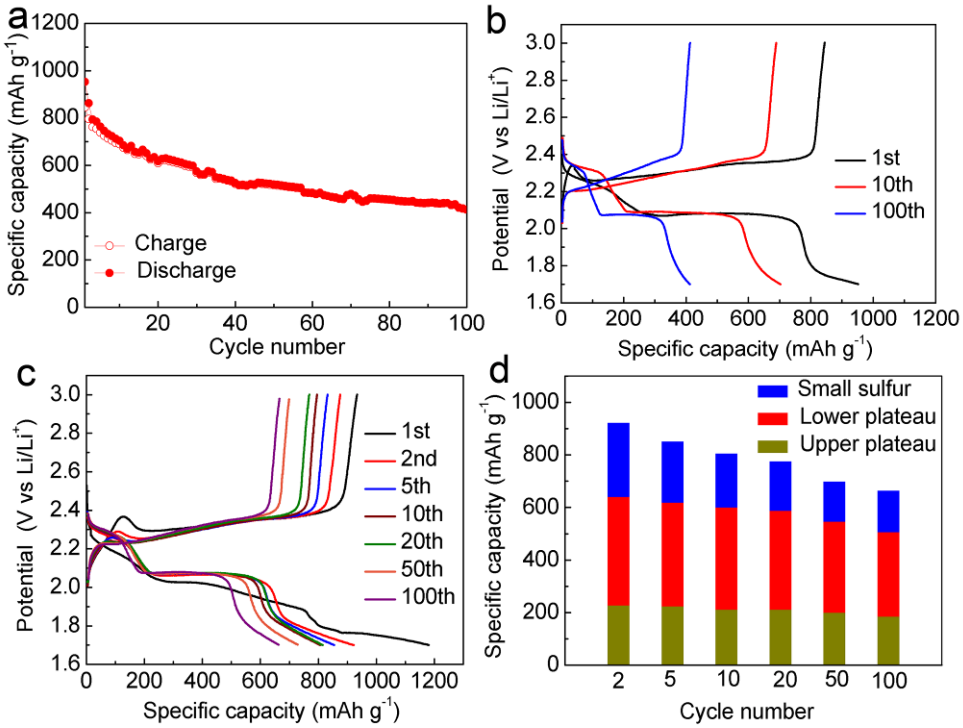

Figure S11. (a) Cycling performance and (b) potential profiles of ZCNs-12/S electrode at 0.5 C. (c) Potential profiles of ZCNs-4/S electrode at 0.5 C. (d) Capacity contribution from higher plateau, lower plateau and small sulfur molecule of ZCNs-4/S electrode.

Table S1. Porous characterizations of ZCNs-4 and ZCNs-12.

Samples	S_{BET} (m^2 g^{-1})	Micro-SSA (m^2 g^{-1})	Pore volume (cm^3 g^{-1})	Micro volume (cm^3 g^{-1})	$\frac{Meso+Macro}{Micro}$
ZCNs-4	1228	639	0.80	0.26	2.46
ZCNs-12	1023	565	0.74	0.23	2.22

References

[S1] Q. Zhang, T. P. Chou, B. Russo, S. A. Jenekhe, G. Z. Cao, *Adv. Funct. Mater.* **2008**, *18*, 1654.

This article is protected by copyright. All rights reserved

Author Manuscript